Supplementary Material

Constructed 3D porous hierarchical micro-flowers WO_3/CdS S-scheme heterojunction for boosting photocatalytic H_2O_2 production and photoelectrochemical cell performance

Yutong Liu[1], Rui Wang[1], Ningning Huang[1], Yingying Guan[1], Meiyu Yang[1], Jiali Yang[1], Shiyu Wang[1], Yang Zhao[1,*], Bolong Jiang[2], Huan Wang[1,*]

[1]College of Chemistry and Chemical Engineering, Northeast Petroleum University, Daqing 163318, China

[2]Innovation Institute for Sustainable Maritime Architecture Research and Technology, Qingdao University of Technology, Qingdao 266000, China

Email: zhaoyang0131@gmail.com;

wanghuan83214@gmail.com

Density functional theory calculation

All calculations were carried out for the material in the framework of Density Functional Theory (DFT) using the Vienna Ab initio Simulation Package (VASP 6.3.0) [1-3]. The generalized gradient approximation (GGA) of the Perdew-Burke-Ernzerhof (PBE) function was used to describe the exchange-correlation energy [4]. The projected augmented wave (PAW) method and pseudopotentials were used to describe the interactions between valence electrons and ions [5]. To ensure the efficiency of the computational results and parallel computing. A 3*3*1 k-point grid under Monkhorst-Pack is used in the optimization process and 450 eV truncation energy is set. The lattice parameters and ionic positions of all crystals were fully relaxed, and the convergence criteria for the total energy of all relaxed atoms and the final force were 10^{-6} eV and 0.03 eV/Å, respectively. The work function (Φ) of WO_3 (001) and CdS (111) was calculated according to the formula of $\Phi = E_V - E_F$, where E_V and E_F stand for the vacuum energy level and Fermi level of the slabs.

Materials

Analytical grade compounds including tungsten chloride (WCl_6), cadmium nitrate tetrahydrate ($Cd(NO_3)_2 \cdot 4H_2O$), and sodium sulfide nonahydrate ($Na_2S \cdot 9H_2O$) were purchased from Aladdin Industrial Corporation. Deionized water (DI) was used during the experiment. All chemicals were analytically pure and did not require further purification.

Material Characterization

The powder X-ray diffraction (XRD) patterns were obtained on a D/MAX-2200,

Japan. Scanning electron microscopy (SEM) and transmission electron microscope (TEM) images were acquired with a Philips XL-30-ESEM-FEG instrument operating at 3 kV and Jem-2100F at an accelerating voltage of 200 kV, respectively. Ultraviolet-visible (UV-vis) diffuse reflection spectra (DRS) were measured on a UV-vis spectrophotometer (UV-2550, Shimadzu) with an integrating sphere attachment, and $BaSO_4$ was used as the reference material. The chemical bond composition was measured by Fourier transform infrared spectrometer (FT-IR, Bruker TENSOR 27). Inductively coupled plasma mass spectrometry (ICP-MS) was conducted on a Thermo Fisher Scientific 6300. X-ray photoelectron spectroscopy (XPS) was taken on the Thermo Fisher Scientific K-Alpha. Electron paramagnetic resonance (EPR) spectra were carried out on a Bruker A300 EPR spectrometer.

Photoelectrochemical measurements

Photoelectrochemical performances were examined by CHI 760E electrochemical workstation (CH Instruments, Chenhua, China) under a three-electrode system in 0.5 M Na_2SO_4 solution by using saturated Ag/AgCl and Pt foil as the reference electrode and counter electrode, respectively. The working electrodes for electrochemical measurements were prepared by dropping the powder samples onto a pre-cleaned indium doped tin oxide (ITO) glass. In detail, 10 mg of photocatalyst was dispersed in an ethanol solution (260 μL) containing 40 μL of Nafion. After dropping the above mixture on ITO followed by drying at 60 °C, the working electrode was obtained. The Mott-Schottky (M-S) curves were measured in the dark at a frequency of 0.5 kHz, respectively. Electrochemical impedance spectra (EIS) were collected at an off-line

potential with frequencies ranging from 105 kHz to 0.1Hz and modulation amplitude of 5.0 mV. The measured potentials (V *vs.* Ag/AgCl) were converted to the reversible hydrogen electrode (RHE) scale according to the Nernst equation: $E_{(RHE)} = E_{(Ag/AgCl)} + 0.0592 \times pH + 0.199$.

Table S1 Detailed composition of as-synthesized formulations.

	Nominal Molar Ratio %	**Ingredients**		**$Cd(NO_3)_2·4H_2O$**	**Na_2S**
		CdS	**WO_3**		
		mmol		mg	mg
WO_3/CdS-4	4	0.018	0.43	5.5	4.32
WO_3/CdS-8	8	0.037	0.43	11.3	8.88
WO_3/CdS-12	12	0.059	0.43	18.2	14.16

Table S2 The results were obtained from N_2 adsorption-desorption isotherms.

Sample	S_{BET} (m^2 g^{-1})	Pore size (nm)	Pore volume (cm^3 g^{-1})
WO_3	71.4461	5.1762	0.09245
CdS	102.5153	8.1665	0.20929
WO_3/CdS-8	78.2110	5.6325	0.11013

Table S3 The content of CdS in the as-prepared WO_3/CdS-8 sample.

Sample	CdS content (mol%)	
	Nominal value	Actual value (ICP-MS)
WO_3/CdS-8	8	7.69

Table S4 A summary of cell performance with different photoanodes.

Photoanode	Power density ($mW \cdot cm^{-2}$)	SECE (%)	Specific capacitance	Specific capacitance is maintained (%)	Ref.
FeO(OH)/BVO	2	0.89			[1]
$BiVO_4$	0.194				[2]
g-C_3N_4	0.156	0.146		2.8 (12 h)	[3]
COCN	0.298	0.248	5900 (3 h)	37.8 (12 h)	[4]
AHCN/AgNCs	0.74	0.42	5975 (2h)	57.2 (12 h)	[5]
Mo-$BiVO_4$	0.18				[6]
PDI/Au	1.07	0.74	5661 (3h)	50.2 (12 h)	[7]
s-PDI/Au	2.36	0.89	49,500 (3h)	52.6 (12 h)	[8]
$BiVO_4$/Ag	0.122				[9]
$BiVO_4$/Ag	2.03	1.75	28,469 (3h)	60 (12 h)	[10]
$BiVO_4/V_2O_5$	0.26				[11]
W-$BiVO_4/V_2O_5$	0.84				[11]
WO_3/CdS	2.97	2.12	29,342 (2h)	51 (12 h)	This work

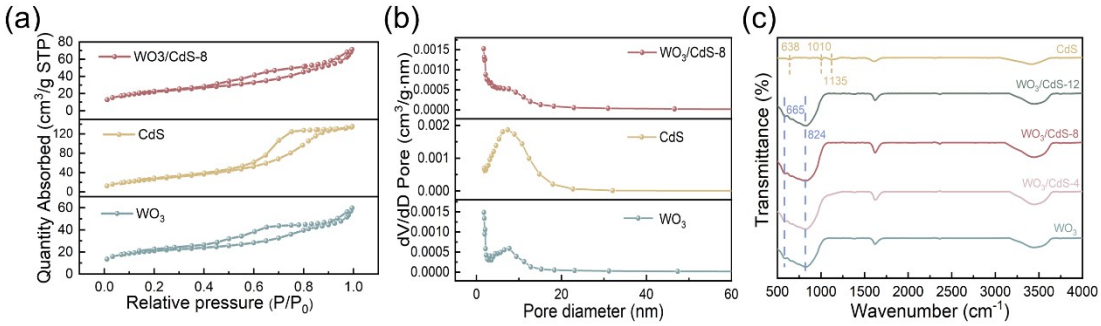

Figure S1. (a) N_2 adsorption/desorption isotherms and (b) corresponding pore-size distribution curves of WO_3, CdS, and WO_3/CdS-8; (c) FT-IR spectra of WO_3, CdS, and WO_3/CdS-x.

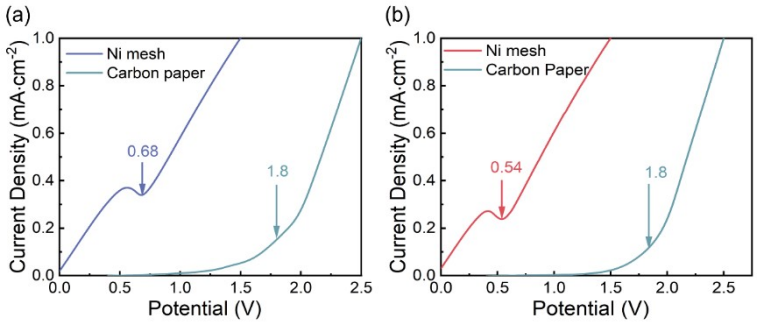

Figure S2. LSV curves of $Fe^{II}Pc/WO_3$/carbon paper electrode combined with (a) WO_3/Ni mesh, and (b) WO_3/CdS-8/Ni mesh, respectively.

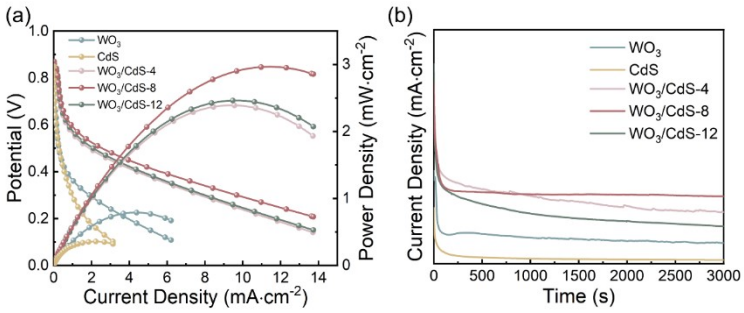

Figure S3. (a) I-V and I-P curves of WO_3, CdS, WO_3/CdS-4, WO_3/CdS-8 and WO_3/CdS-12-based cells; (b) Specific capacitance of the WO_3, CdS, WO_3/CdS-4, WO_3/CdS-8 and WO_3/CdS-12-based cells after 0.5 h light irradiation for H_2O_2 storage.

Table S5 Specific capacitance of the WO_3, CdS, WO_3/CdS-4, WO_3/CdS-8 and WO_3/CdS-12-based cells after 0.5 h light irradiation for H_2O_2 storage.

Sample	Specific capacitance (irradiated 0.5h)
WO_3	9463 mF cm^{-2}
CdS	2005 mF cm^{-2}
WO_3/CdS-4	23728 mF cm^{-2}
WO_3/CdS-8	25989 mF cm^{-2}
WO_3/CdS-12	18240 mF cm^{-2}

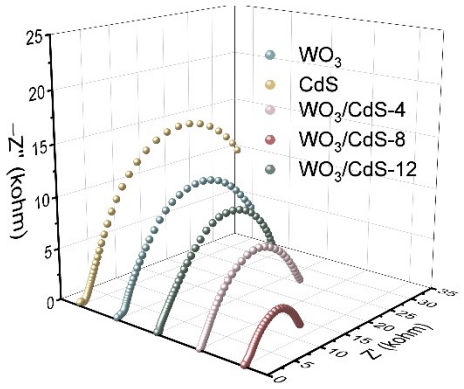

Figure S4. Electrochemical impedance spectra (EIS) of WO_3, CdS, WO_3/CdS-4, WO_3/CdS-8 and WO_3/CdS-12.

References

1 K. Mase, M. Yoneda, Y. Yamada and S. Fukuzumi, *ACS Energy Lett.*, 2016, 1, 913–919.

2 X. Shi, Y. Zhang, S. Siahrostami and X. Zheng, *Adv. Energy Mater.*, 2018, 8, 1801158.

3 N. Liu, M. Han, Y. Sun, C. Zhu, Y. Zhou, Y. Zhang, H. Huang, V. Kremnican, Y. Liu, Y. Lifshitz and Z. Kang, *Energy Environ. Sci.*, 2018, 11, 1841–1847.

4 X. Li, H. Cong, R. Wang, Y. Wang, Z. Nie, Q. Jing, Y. Zhao, H. Song, H. Wang, *J. Power Sources.*, 2022, 532, 231368.

5 R. Wang, Q. Jing, X. Li, S. Wang, Y. Zhao and H. Wang, *J. Power Sources.*, 2024, 608, 234654.

6 Y. Li, X. Li, M. Yang, R. Wang, J. Li, G. Cui, Y. Zhao and H. Wang, *Electrochim. Acta*, 2024, 495, 144491.

7 X. Sun, J. Chen, J. Zhai, H. Zhang and S. Dong, *J. Am. Chem. Soc.*, 2022, 9, 23073–23080.

8 R. Wang, M. Yang, J. Yang, Y. Li, Y. Zhao, B. Jiang and H. Wang, *ACS Appl. Nano Mater.*, 2024, 7, 21436–21444.

9 N. Huang, X. Li, T. Xing, F. Sun, M. Yang, J. Yang, Y. Zhao and H. Wang, *Energy Fuels*, 2024, 38, 19029–19037.

10 Z. Miao, R. Wang, X. Li, F. Sun, M. Ge, N. Huang, Y. Zhao, Z. Chang and H. Wang, *J. Power Sources.*, 2025, 629, 235998.

11 T.S. Andrade, B.A.C. Sa, F.G.E. Nogueira, L.C.A. Oliveira and M.C. Pereira, *J. Appl. Electrochem.*, 2023, 53, 435–444.